
The Discrete Charm of the MLP: Binary Routing of Continuous Signals in Transformer Feed-Forward Layers

Peter Balogh
palexanderbalogh@gmail.com

“It just happened that no one else was familiar with both fields at the same time.”
—Claude Shannon

Abstract

We show that MLP layers in transformer language models perform *binary routing of continuous signals*: the decision of whether a token needs nonlinear processing is well-captured by binary neuron activations, even though the signals being routed are continuous. In GPT-2 Small (124M parameters), we find that specific neurons implement a consensus architecture—seven “default-ON” neurons and one exception handler (N2123 in Layer 11) that are 93–98% mutually exclusive—creating a binary routing switch. A cross-layer analysis reveals a developmental arc: early layers (L1–3) use single gateway neurons to route exceptions without consensus quorums; middle layers (L4–6) show diffuse processing with neither gateway nor consensus; and late layers (L7–11) crystallize full consensus/exception architectures with increasing quorum size (1→3→7 consensus neurons). Causal validation confirms the routing is functional: removing the MLP at consensus breakdown costs 43.3% perplexity, while at full consensus removing it costs only 10.1%—exceeding a 4× difference. Comparing binary vs. continuous features for the routing decision confirms that binarization loses essentially no information (79.2% vs. 78.8% accuracy), while continuous activations carry additional magnitude information ($R^2 = 0.36$ vs. 0.22). This binary routing structure *explains* why smooth polynomial approximation fails: cross-validated polynomial fits (degrees 2–7) never exceed $R^2 = 0.06$ for highly nonlinear layers. We propose that the well-established piecewise-affine characterization of deep networks [Balestriero & Baraniuk, 2018] can be complemented by a *routing* characterization: along the natural data manifold, the piecewise boundaries implement binary decisions about which tokens need nonlinear processing, routing continuous signals through qualitatively different computational paths.¹

1 Introduction

1.1 The Smooth Function Framing

The standard view of transformer MLPs treats them as function approximators. The residual stream presents what looks like a function-approximation problem: the MLP receives a 768-dimensional input and must produce a 768-dimensional output, pointwise, for each token position. It is natural to frame this as curve-fitting: the MLP uses its 3072 piecewise-linear (GELU) neurons to approximate

¹Code and data available at <https://github.com/pbalogh/discrete-charm-mlp>

whatever smooth function maps inputs to outputs along the data manifold. The universal approximation theorem assures us this is possible; the question becomes how efficiently the network achieves it.

The most elegant formalization of this view is Balestriero & Baraniuk [2018], who prove rigorously that deep networks with piecewise-linear activations compute continuous piecewise-affine spline functions—a result that connects neural networks to classical approximation theory. Under the spline view, the network partitions its input space into polytopes and fits an affine (degree-1) function within each. This characterization is mathematically precise and correct: every forward pass *does* trace a path through a piecewise-affine partition.

We take this characterization as our starting point and ask a complementary question: what kind of *computation* does the piecewise structure implement? The spline framework tells us the MLP partitions input space into regions with different affine maps. But it does not tell us whether those regions reflect smooth variation along the data manifold—the MLP approximating a continuous function with increasing local resolution—or whether they reflect discrete *decisions*: binary conditions that route tokens to qualitatively different processing.

Consider a concrete analogy. A 2D shape—say, the infinity symbol (∞)—projected onto a 1D number line collapses points near the crossing: distinct locations on the upper and lower loops map to the same coordinate. The MLP must resolve this ambiguity. Under the smooth function framing, we expect it to do so by tracing the curve through the intersection—separate branches, each locally smooth, recoverable by the right clustering or polynomial fit. We find instead that it does so by *flipping a switch*: upper or lower, a binary decision.

The MLP’s $4\times$ width expansion temporarily provides more dimensions, and the nonlinear activation creates the region boundaries—but the character of those boundaries turns out to be discrete routing, not smooth approximation.

1.2 The Kolmogorov Connection

The Kolmogorov representation theorem guarantees that any continuous multivariate function can be decomposed into compositions of univariate functions and addition. An MLP literally implements this: linear combination \rightarrow pointwise nonlinearity \rightarrow repeat. But the theorem says nothing about the *character* of the univariate functions needed. If the underlying computation is low-degree polynomial, the MLP is wastefully approximating it with thousands of linear pieces. If it is high-degree or non-polynomial, the piecewise approximation may be the most efficient representation available. And if the computation is fundamentally discrete—a set of binary routing decisions—then the piecewise structure is not approximating anything at all; it is implementing a switching network.

We set out to determine which case holds in practice by looking for smooth structure in the nonlinear component, and simultaneously looking for discrete structure in the neuron activations. The smooth structure is absent; the discrete structure is present and interpretable.

1.3 An Analogy: Shannon’s Switch

In 1937, Claude Shannon showed that relay switches—continuous electromechanical devices—could implement Boolean algebra: each switch routes current or blocks it, and any arrangement of switches implements a logical expression [Shannon, 1938]. Before Shannon, engineers analyzed relay circuits using the continuous mathematics of current flow and impedance. The discrete ON/OFF behavior was a practical detail, not a theoretical framework. Shannon’s insight was that the continuous properties could be *ignored entirely*: all the computational content lives in the switching pattern, and the continuous current is just a substrate.

Shannon could afford this simplification because relay current genuinely carried no computational information—5mA and 50mA both meant ON. We find that the MLP presents a more interesting case: the *routing decision* (which tokens need nonlinear processing) is binary, but the *signal being routed* is continuous, and both carry essential information. A GELU neuron, in its trained operating regime, is approximately zero for strongly negative pre-activations and approximately the identity for strongly positive ones. Each neuron effectively evaluates a binary routing predicate: *should feature j ’s contribution pass through to the output?* The full MLP computes 3072 such routing decisions in

parallel, then linearly combines the results:

$$\text{MLP}(x) = W_{\text{out}} \cdot [\text{GELU}(W_{\text{in}} x + b_{\text{in}})] + b_{\text{out}} \tag{1}$$

This is well-known—it is how ReLU-family activations work. Our contribution is not the observation that GELU has a near-zero and near-linear regime, but the empirical finding that *specific neurons in trained networks* exploit this to implement interpretable binary routing with structure that goes far beyond what their marginal firing rates would predict—and that this routing decision, not the continuous activation magnitudes, determines whether the MLP’s computation matters.

To be precise about what we mean by “binary routing” in this context: we do not claim that GELU neurons are ideal binary gates, nor that the MLP implements a formally specified Boolean algebra. We observe that (a) individual neurons operate in a near-binary regime for most tokens on the data manifold, (b) specific neurons exhibit 93–98% mutual exclusivity that cannot be explained by their marginal firing rates under independence (§4), and (c) the binarized activation patterns are semantically coherent and predict the MLP’s output norm. We use “binary routing” as a descriptive characterization of this emergent structure—a framework for understanding what the piecewise-affine spline *computes*, complementing the spline framework’s description of how it computes.

The analogy to Shannon is therefore one of *starting point*, not destination. Shannon showed that treating switches as signal routers opened a productive design theory; he could then discard the continuous signal as irrelevant substrate. We suggest that treating GELU neurons as binary routers of continuous signal opens a similar interpretive framework—but in the MLP, unlike in Shannon’s relays, the continuous signal *cannot* be discarded. Binarization captures the routing decision with essentially no loss (79.2% vs. 78.8% accuracy, §4), but continuous activation magnitudes carry additional information about *how much* correction to apply ($R^2 = 0.36$ vs. 0.22). The MLP is a synthesis that neither the purely digital nor the purely analog framing captures: binary routing of continuous signals, where both the routing logic and the signal magnitude are computationally essential.

2 Method

All experiments use GPT-2 small (124M parameters, 12 layers, 3072 MLP hidden neurons per layer) [Radford et al., 2019] with original OpenAI weights on WikiText-103 [Merity et al., 2016]. Results are validated at both 50K and 500K tokens (50.4% vocabulary coverage at 500K).

2.1 Polynomial Probing

For each MLP layer, we collect input–output pairs along the data manifold:

1. Run text through the model, hooking each MLP to capture input x_i (residual stream after attention) and output y_i for each token position i .
2. Fit the best linear approximation $\hat{y}_i = Wx_i + b$ via least squares. The residual $\delta_i = y_i - \hat{y}_i$ isolates the purely nonlinear component.
3. Project inputs to $k = 50$ PCA dimensions (retaining >95% of variance), construct polynomial features up to degree $d \in \{2, 3, 4, 5, 6, 7\}$, and fit Ridge regression ($\alpha = 1.0$) predicting PCA-compressed δ . Results are stable across $k \in \{10, 20, 50, 100\}$ and $\alpha \in \{0.1, 1, 10, 100\}$ (Appendix C).
4. Cross-validate: fit on 70% of tokens, evaluate on held-out 30%.

2.2 Branch Detection

The smooth function framing does not require a single polynomial to cover all tokens—the spline characterization explicitly predicts different affine maps in different regions. Our branch detection experiments therefore ask a stronger question: even allowing *multiple* smooth subpopulations, each with its own polynomial (potentially at different degrees), can we find any subset of tokens where the nonlinear residual has smooth structure?

We cluster high- $\|\delta\|$ tokens and fit polynomials per cluster using five methods: KMeans on input activations, KMeans on delta directions ($\delta_i/\|\delta_i\|$), KMeans on joint input + delta, spectral clustering

Table 1: Cross-validated polynomial R^2 on high- $\|\delta\|$ tokens (top 10%), 100K tokens.

Layer	Deg 2	Deg 3	Deg 4	Deg 5	Deg 6	Deg 7
L9	0.062	0.041	0.041	0.034	0.022	0.022
L11	0.170	0.248	0.260	0.262	0.202	0.208

Table 2: Branch detection: polynomial R^2 after clustering Layer 9 high- $\|\delta\|$ tokens. Five methods, all cross-validated. No method finds polynomial-tractable subsets.

Clustering Method	Avg Val R^2	Best Cluster R^2
KMeans (input)	-0.068	0.021
KMeans (delta dir.)	-0.023	0.008
KMeans (joint)	-0.061	0.020
Spectral (delta dir.)	-2.182	0.013
UMAP + KMeans	-0.030	-0.021

on delta directions, and UMAP + KMeans on delta directions. All evaluations use held-out data assigned to clusters via nearest centroid.

2.3 Binary Feature Extraction

We partition tokens into three regimes by $\|\delta_i\|$ percentile:

- **Linear** (bottom 25%): MLP operates linearly; no binary conditions fire.
- **Barely nonlinear** (50th–70th percentile): Few conditions distinguish these from linear.
- **Highly nonlinear** (top 5%): Full binary routing logic engaged.

For each of the 3072 hidden neurons, we compare firing rates (GELU output > 0.1) across groups and identify neurons whose firing rate shifts most between regimes. We then binarize the top- k neurons and analyze the resulting bit patterns as binary routing logics.

3 Results I: Polynomials Fail Categorically

Cross-validated polynomial fits (degrees 2–7, $k = 50$ PCA dimensions, Ridge $\alpha = 1.0$) on the nonlinear residual δ capture at most $R^2 = 0.06$ for Layer 9 and $R^2 = 0.26$ for Layer 11 (Table 1). Higher degrees *decrease* performance for L9, indicating overfitting rather than underfitting. Context augmentation (± 3 tokens) provides no improvement. Results are stable across PCA dimensions and regularization strengths (Appendix C).

Critically, even allowing *multiple* smooth subpopulations fails. We cluster high- $\|\delta\|$ tokens using five methods (KMeans on input, delta direction, and joint features; spectral clustering; UMAP+KMeans) and fit per-cluster polynomials. No method finds any subset where a cubic generalizes: the best cluster validation R^2 across all methods is 0.021 (Table 2). The nonlinearity is not a mixture of smooth functions.

The one exception is paragraph boundary tokens ($\backslash\text{n}\backslash\text{n}$) at Layer 11, where a cubic achieves $R^2 = 0.45$ on validation and replacing the MLP’s output with the cubic prediction *improves* perplexity by 0.1% (within noise given the small token count; the point is directional, not that the cubic is genuinely superior). This is the exception that clarifies the rule: paragraph boundaries trigger a single consistent activation pattern—one routing condition with one outcome—that happens to resemble a low-degree polynomial. For any token class with more complex routing logic, the approximation fails. Sub-clustering function words into 2–16 groups confirms this: fit R^2 grows with clusters but validation R^2 stays negative (pure overfitting).

Table 3: Layer 11 neurons with largest firing-rate shift between linear-default (bottom 25% by $\|\delta\|$) and highly-nonlinear (top 5%) tokens. 500K WikiText-103 tokens. Semantic roles are descriptive labels based on inspecting the top-firing tokens for each neuron; they are not independently validated (see §5.8 for discussion).

Neuron	Linear %	High-NL %	Δ	Semantic Role
2123	0.4%	80.7%	+80.3	Exception handler
2	99.1%	26.1%	-73.0	General punctuation
2361	93.2%	22.6%	-70.6	Subordinate clauses
2460	86.1%	19.8%	-66.3	Content words
2928	80.4%	16.2%	-64.2	Default-ON
1831	79.9%	17.7%	-62.2	Default-ON
1245	82.3%	20.8%	-61.5	Default-ON
2600	74.7%	16.1%	-58.6	Default-ON

4 Results II: Binary Routing Structure

4.1 From Activation Properties to Learned Structure

That GELU has a near-zero and near-linear regime is a property of the activation function. What is *not* a property of the activation function is the specific pattern of co-activation and mutual exclusivity that emerges in trained weights. A reviewer might reasonably ask: “Aren’t you just rebranding how ReLU-family activations work?” The answer depends on whether the binarized patterns carry structure beyond what marginal firing rates predict.

Consider neuron N2123, which fires for 11.3% of tokens overall, and neuron N2 (a consensus neuron), which fires for 78.3%. Under independence, they should co-fire for $0.113 \times 0.783 = 8.85\%$ of tokens, or $\sim 44,200$ of 500K. The observed co-firing count is 18,259 tokens—a 58.7% reduction from the independence baseline. This pattern holds across all seven consensus neurons (Table 4). The mutual exclusivity is not a consequence of GELU’s shape; it is a property of the *learned weight vectors* w_{2123} and w_2 being oriented to define complementary half-spaces in the 768-dimensional input.

The question is whether this learned complementary structure is better described as “smooth function approximation with cancellation” or as “binary routing of continuous signals through different computational paths.” The evidence in this section supports the latter.

4.2 Neuron Forensics

For Layer 11 at 500K tokens, we identify neurons whose firing rates differ most between the linear-default and highly-nonlinear regimes:

The pattern is unmistakable. Seven neurons are **default-ON**: they fire for 74–99% of linear-default tokens and drop to 15–26% for highly-nonlinear tokens. One neuron—N2123—does the opposite: silent for 99.6% of linear tokens, firing for 80.7% of highly-nonlinear ones. (Note: this 80.7% is the fire rate among the top-5% most nonlinear tokens by $\|\delta\|$; the related figure of 94.7% in §4.4 is the fire rate at 0/7 consensus. Both measure the same phenomenon—N2123 activating when the MLP needs nonlinear processing—but using different regime definitions.)

4.3 Neuron 2123: The Exception Handler

N2123 is 93–98% mutually exclusive with each of the seven default-ON neurons (Table 4). This is not a statistical tendency—it is a hard IF/ELSE in the learned weights.

Statistical significance. Under independence, N2123 (11.3% fire rate) and N2 (78.3%) should co-fire for $\sim 44,200$ of 500K tokens; we observe 18,259 ($\chi^2 > 10,000$, $p < 10^{-300}$). All seven pairs show similar significance. The exclusivity is not a statistical tendency—it is a near-deterministic property of the learned weight geometry.

Threshold robustness. The binarization threshold of 0.1 is not critical. Table 5 shows that the consensus gradient is perfectly monotonic at all five thresholds tested (0.01–1.0), with exclusivity

Table 4: Mutual exclusivity between N2123 and the seven default-ON neurons. “Both fire” counts tokens where both GELU outputs exceed 0.1. 500K tokens.

Neuron Pair	Both Fire	Union Fire	Exclusivity
2123 vs N2	18,259	429,427	95.7%
2123 vs N2361	21,792	394,781	94.5%
2123 vs N2460	14,199	436,944	96.8%
2123 vs N2928	18,846	473,231	96.0%
2123 vs N1831	8,522	394,259	97.8%
2123 vs N1245	12,471	439,196	97.2%
2123 vs N2600	22,756	317,606	92.8%

ranging from 94.1% to 99.3%. The gradient weakens at high thresholds (rate range drops from 96.4pp at 0.01 to 23.0pp at 1.0) because fewer neurons qualify as “firing,” but the monotonic structure persists. The binary routing characterization is robust to the choice of threshold.

Table 5: **Threshold sensitivity.** Consensus structure at five GELU binarization thresholds. Layer 11, 500K tokens, forward hooks. All thresholds produce monotonic gradients.

Threshold	N2123 FR	Def-ON FR	Exclusivity	Monotonic	Range
0.01	13.1%	79.2%	94.1%	✓	96.4pp
0.05	12.2%	77.2%	95.0%	✓	95.9pp
0.10	11.3%	74.5%	95.8%	✓	94.3pp
0.50	7.9%	50.9%	98.5%	✓	66.3pp
1.00	6.2%	23.4%	99.3%	✓	23.0pp

Random neuron control. Is this structure special, or would any 7+1 neuron split produce similar results? We test 1,000 random trials: 7 high-firing neurons (>50% rate) + 1 low-firing neuron (1–10% rate), mimicking the structural form of the real consensus. The real neurons’ consensus gradient—a 94.3 percentage-point range in exception-handler firing rate from 0/7 to 7/7—was matched by **zero** of 1,000 random trials (best: 53.5pp). The real norm ratio (2.77×) was exceeded by only 10/1,000 (1.0%). Exclusivity alone is less discriminative (220/1,000 beat 95.8%), confirming that high mutual exclusivity between high- and low-firing neurons is partly a base-rate phenomenon—but the *gradient structure* that links consensus to both exception-handler firing and output norm is specific to the learned neurons, not an artifact of firing-rate distributions.

Random weight control. Is the consensus structure a property of the GPT-2 architecture or of the learned weights? We run the identical analysis on a randomly initialized (untrained) GPT-2 Small. With random weights, N2123 fires at ~78% regardless of consensus level (no gradient), the norm ratio is 1.0× (uniform norm of 2.0), and average exclusivity drops to 81.7%. The consensus architecture is entirely absent in the untrained model, confirming that it is a property of the *learned weight geometry*, not of the GELU activation function or the MLP architecture.

4.4 Two Regimes: The Consensus Gradient

Figure 1 presents the central result of this paper (full data in Appendix Table 9). When none of the 7 consensus neurons fire, N2123 activates for 94.7% of tokens and MLP output norm reaches 194.1 (2.8× the consensus-present norm of 70.0). When all 7 agree, N2123 fires for 0.5% and the MLP output is minimal—close to the linear default.

The gradient is perfectly monotonic: 10,000 bootstrap resamples of the 500K-token dataset produce a 95% CI of [93.8, 94.7]pp for the gradient range, [2.73, 2.81]× for the norm ratio, and [95.8, 95.9]% for average exclusivity, with monotonicity preserved in 100% of bootstrap samples.

N2123 is not a feature detector in the usual sense. It is a **consensus monitor**: it detects that the standard neural committee has failed to agree, and triggers the full nonlinear computation as a fallback. This is software architecture—fast path / slow path—emerging from gradient descent.

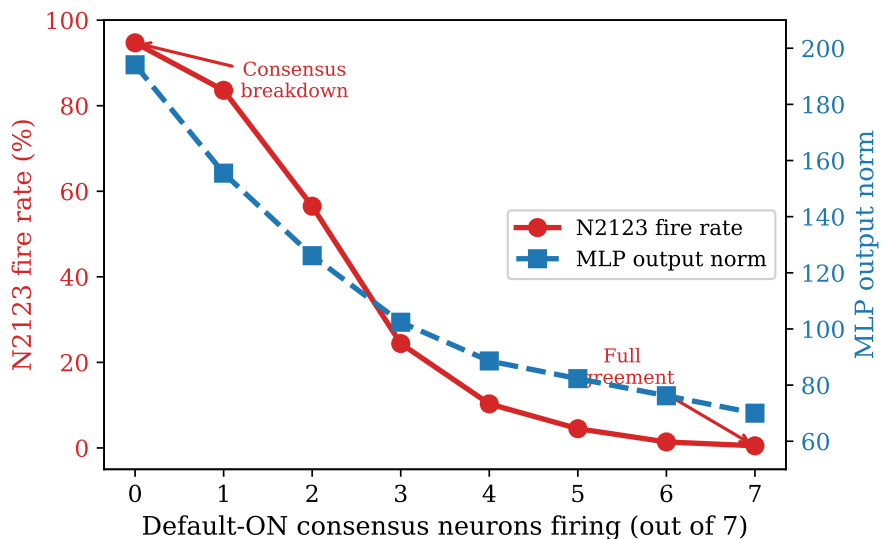


Figure 1: **Two Regimes.** N2123 fire rate (red, left axis) and MLP output norm (blue, right axis) as a function of default-ON consensus neuron count. The gradient is perfectly monotonic: consensus breakdown triggers the exception handler and $2.8\times$ output norm. 500K WikiText-103 tokens, GPT-2 Small Layer 11.

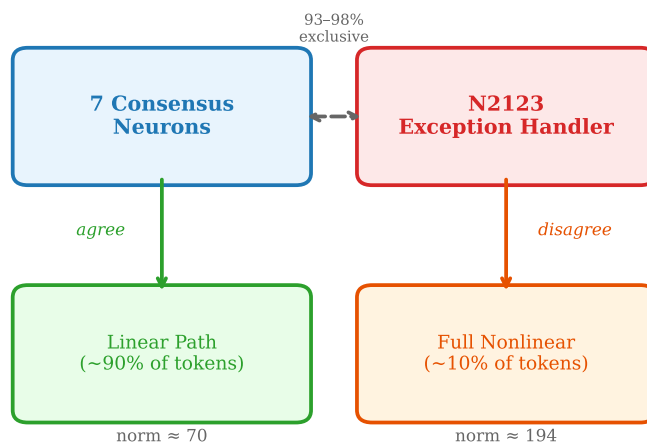


Figure 2: **Exception handler architecture** emerging from learned weights in Layer 11. Seven default-ON consensus neurons and N2123 are 93–98% mutually exclusive. When consensus holds, the MLP operates near-linearly (norm ≈ 70); when it breaks down, N2123 fires and triggers full nonlinear computation (norm ≈ 194).

Note that the “fast path” is not literally faster in hardware: all 3072 neurons compute their activations and multiply through W_{out} regardless. The distinction is *informational*. When consensus holds, the 3072 neuron votes approximately cancel—the MLP’s net output is small, and a simple linear transform would have produced the same result. The mechanism table (§4.9) confirms this: at full consensus, the MLP’s correct-token boost drops below $1.0\times$, meaning its residual intervention is noise rather than signal. When consensus fails, the votes stop canceling, the net output is large and specific, and the result genuinely depends on which neurons fired. The same continuous signals are now routed through a qualitatively different computation. The expensive processing is “expensive” not because it costs more FLOPs, but because it **could not have been achieved more cheaply**.

4.5 Binary Patterns as Pseudocode

Binarizing the top 8 discriminative neurons (ranked by $|\Delta\text{fire-rate}|$ between barely-nonlinear and linear-default tokens using the nonlinearity delta metric) and encoding each token as an 8-bit pattern, we identify patterns enriched 10–41 \times in barely-nonlinear tokens compared to linear-default tokens:

```
# Top 8 neurons: N458, N2600, N2032, N2821, N1010, N3, N309, N1829
# (ranked by |fire-rate difference|, nonlinearity delta, 500K tokens
)

# Pattern 00010000 (41.1x enriched): closed-class function words
IF N2821 AND NOT(458,2600,2032,1010,3,309,1829):
  # determiners, conjunctions, copulas, auxiliaries
  # 'a', 'and', 'is', 'the', 's', 'had'
  apply_function_word_correction()

# Pattern 01010000 (13.9x enriched): subject pronouns / auxiliaries
IF N2600 AND N2821 AND NOT(458,2032,1010,3,309,1829):
  # subject-position pronouns and auxiliaries
  # 'he', 'she', 'She', 'it', 'He', 'had'
  apply_subject_correction()

# Pattern 00010001 (17.8x enriched): past-tense/narrative function
words
IF N2821 AND N1829 AND NOT(458,2600,2032,1010,3,309):
  # function words in past-tense narrative contexts
  # 'was', 'and', 'the', 'to', 'his', 'a'
  apply_narrative_correction()

ELSE:
  use_linear_default()
```

Figure 3: Extracted binary logic from Layer 11 MLP (simplified). Pattern enrichment validated at 500K tokens using the nonlinearity delta (least-squares residual) metric. Full pattern table in supplementary material.

The patterns reveal **grammatical structure**: N2821 (fires MORE for barely-nonlinear tokens; bias +0.27, default OFF) acts as a gateway—it fires in 19 of the top 20 enriched patterns (full table in supplementary material), gating access to nonlinear correction. The remaining 7 neurons (all firing LESS for barely-nonlinear tokens) subdivide the correction by grammatical category. Pattern 00010000 (N2821 alone, all others silent) captures the broadest class—closed-class function words (determiners, conjunctions, copulas, auxiliaries)—at 41 \times enrichment. Additional neurons narrow within this class: adding N2600 selects subject pronouns (*he, she, it*; 13.9 \times), while adding N1829 selects function words in past-tense narrative contexts (*was, his*; 17.8 \times). The MLP is implementing a soft part-of-speech tagger composed from binary feature detectors.

Binarization preserves routing information. To test whether the binary framing discards useful signal, we compare binarized vs. continuous activations of the same 8 neurons for predicting MLP importance. For the binary routing decision (top-25% nonlinearity vs. rest), logistic regression achieves 79.2% with binary features and 78.8% with continuous—binarization loses essentially nothing. For predicting the continuous output norm (Ridge regression), continuous features win ($R^2 = 0.36$ vs. 0.22), indicating that activation magnitude carries additional information about *how much* nonlinearity is needed, even after the binary routing decision is made. The routing decision itself, however, is well-captured by binary features alone.

4.6 Decision Tree Validation

We fit a decision tree predicting nonlinearity quintile from binarized neuron activations. A depth-5 tree achieves 34.7% validation accuracy on 5 classes (25.2% baseline). More tellingly, a depth-3 binary tree (LINEAR_OK vs NEEDS_MLP) achieves **80.7%** validation accuracy (74.7% baseline),

confirming that the linear/nonlinear routing decision is well-captured by a small number of binary conditions.

4.7 Consensus Structure Across All Layers

We repeat the consensus analysis for all 12 layers of GPT-2 Small using a more rigorous protocol: 500K tokens, with the nonlinearity delta ($\|\delta\|$, the least-squares residual norm) as the regime-assignment metric. For each layer, we identify exception-handler neurons, consensus quorum neurons, and gateway neurons (those firing preferentially for barely-nonlinear tokens, gating access to nonlinear correction). This larger-scale analysis reveals that the consensus architecture is *not* uniformly present—it develops through depth in three distinct phases.

Table 6: **Three-phase developmental arc across GPT-2 Small.** Consensus/exception architecture emerges through depth. Mean Δ : average nonlinearity delta (higher = more nonlinear computation). #Cons: number of consensus neurons identified. Gateway: neuron firing in most top-enriched binary patterns. 500K WikiText-103 tokens.

Layer	Phase	Mean Δ	Exception	Excl.	#Cons	Gateway	Monotonic
0	Scaffold	10.9	N2053 (9%)	94%	1	—	✓
1	Scaffold	8.2	—	—	—	N2882 (19/20)	×
2	Scaffold	11.4	—	—	—	N2380 (20/20)	×
3	Scaffold	11.7	—	—	—	N746 (17/20)	×
4	Diffuse	11.9	—	—	—	—	×
5	Diffuse	13.9	—	—	—	—	×
6	Diffuse	16.0	—	—	—	—	×
7	Decision	19.2	N1990 (8%)	99%	1	N690 (15/20)	✓
8	Decision	22.8	N589 (27%)	~85%	3	N2406 (15/20)	✓
9	Decision	28.1	N1999 (15%)	—	—	N2523 (15/20)	✓
10	Decision	35.9	N1858 (20%)	~85%	3	—	✓
11	Decision	44.1	N2123 (10%)	93–98%	7	N2821 (15/20)	✓

The three phases are:

Scaffold layers (L0–L3). These layers have low nonlinearity deltas (8–12) and process most tokens near-linearly. Layers 1–3 each exhibit a single *gateway* neuron—a neuron that fires preferentially for barely-nonlinear tokens, appearing in 17–20 of the top 20 enriched binary patterns—but no consensus quorum. Layer 0 is the exception: it shows a single consensus neuron with 94% exclusivity against its exception handler (N2053), making it structurally closer to the decision layers. The scaffold layers route exceptions through individual gateway neurons rather than committee voting.

Diffuse layers (L4–L6). These layers show neither gateway neurons nor consensus structure. The nonlinear computation is distributed across many neurons without identifiable routing bottlenecks. This is consistent with these layers performing distributed feature transformation that does not decompose cleanly into binary routing decisions.

Decision layers (L7–L11). The consensus/exception architecture crystallizes here, with increasing complexity through depth. Layer 7 has a single consensus neuron with 99% exclusivity; Layer 8 has three consensus neurons at ~85% exclusivity; Layer 11 has the full seven-neuron quorum at 93–98%. All five decision layers show perfectly monotonic consensus gradients. Among layers with identifiable consensus, the quorum size generally increases with depth (1→3→3→7), though L9–10 show exception/gateway structure without clear consensus quorums, breaking strict monotonicity.

This developmental arc is a stronger finding than uniform consensus across all layers. It suggests that binary routing *emerges* through depth as the model transitions from simple feature extraction (scaffold), through distributed transformation (diffuse), to complex decision-making where the consensus/exception architecture provides the interpretable routing structure detailed in the preceding sections.

4.8 Causal Validation: MLP Ablation by Consensus Level

The correlational evidence—N2123’s firing rate, output norms, mutual exclusivity—establishes that the consensus structure exists in the weights. But does it matter causally? We test this directly: for each consensus level, we zero the *entire* Layer 11 MLP output for tokens at that level and measure the perplexity impact.

Table 7: **Causal validation.** Perplexity impact of removing the Layer 11 MLP for tokens at each consensus level. Losses at position t (predicting token $t+1$) are grouped by the consensus level at position t . 500K WikiText-103 tokens, GPT-2 Small. Token counts are slightly lower than Table 9 (499,224 vs. 499,712) because the last token of each 1024-token sequence has no next-token loss.

Consensus	N tokens	Base PPL	No-MLP PPL	$\Delta\%$
0 / 7	11,351	5.4	7.7	+43.3%
1 / 7	19,110	7.3	9.7	+32.6%
2 / 7	19,121	12.2	16.1	+31.6%
3 / 7	26,169	20.3	25.7	+26.7%
4 / 7	52,994	19.5	23.3	+19.1%
5 / 7	95,194	39.1	46.0	+17.6%
6 / 7	145,927	49.3	56.5	+14.7%
7 / 7	129,358	39.5	43.5	+10.1%
All	499,224	32.3	37.7	+16.9%

The gradient is perfectly monotonic (Table 7). When all 7 consensus neurons agree, removing the MLP costs 10.1%—still measurable, but far less than at breakdown. When none agree, removing the MLP costs 43.3%. The ratio between breakdown and consensus impact exceeds $4\times$.

Note the inverted base PPL: consensus-breakdown positions (0/7) have *low* base perplexity (5.4) because these are function words (“a”, “the”, “to”) whose *next* token is highly predictable. The consensus level reflects the MLP’s processing difficulty at position t , while the loss measures prediction quality for token $t+1$. The key finding is the *delta gradient*: the MLP’s contribution to next-token prediction is $4\times$ larger at consensus breakdown than at full consensus, confirming that the consensus structure predicts functional importance.

4.9 The Causal Mechanism: What the MLP Computes

The ablation tells us *whether* the MLP matters; we can also measure *what it does*. Table 8 shows how the MLP modifies the output distribution at each consensus level, measured as KL divergence between the full-model and MLP-ablated logits, the probability boost for the correct next token, and the rank improvement.

Table 8: **MLP mechanism by consensus level.** KL divergence between full and no-MLP logits, correct-token probability with and without MLP, and rank change. 500K WikiText-103 tokens, GPT-2 Small Layer 11.

Consensus	N	KL div	Boost	Δ Rank
0 / 7	11,351	0.414	1.15\times	-33.9
1 / 7	19,110	0.338	1.08 \times	-45.1
2 / 7	19,121	0.315	1.05 \times	-22.4
3 / 7	26,169	0.290	1.03 \times	-12.3
4 / 7	52,994	0.238	0.97 \times	-8.4
5 / 7	95,194	0.222	0.94 \times	-9.9
6 / 7	145,927	0.206	0.90 \times	-13.4
7 / 7	129,358	0.212	0.85 \times	+4.9

Two patterns emerge. First, the KL divergence gradient is monotonic: the MLP reshapes the output distribution substantially at consensus breakdown (KL = 0.414) and progressively less as consensus

increases (KL = 0.212 at 7/7). The consensus structure tracks a real gradient in how much the MLP modifies the next-token distribution.

Second, and more revealing, there is a *dissociation* between the MLP’s effect on the overall distribution (KL) and its effect on the correct token (boost). Even at peak importance (0/7), the MLP’s average boost to the correct token is modest (1.15×), while its KL divergence is large (0.414). This means the MLP’s computation at consensus breakdown is primarily *distributional*: it reshapes probability mass across many tokens rather than concentrating it on the correct one. The 4× perplexity gradient (Table 7) reflects this broad distributional reshaping, not a targeted boost to the correct token. At full consensus, even this distributional effect fades: the boost crosses below 1.0× from 4/7 onward, and rank worsens at 7/7 (+4.9), indicating that the residual MLP intervention is not merely unnecessary but mildly counterproductive—noise rather than signal.

This reveals the causal mechanism behind the Two Regimes. At consensus breakdown, the MLP performs genuinely useful distributional computation: resolving ambiguity across the full vocabulary that the attention heads could not. At consensus, this computation has no useful target—the MLP still fires (all 3072 neurons compute) but its output is diffuse and slightly harmful. The selective linearization hypothesis of Balogh [2026b] is thus confirmed with a nuance: consensus tokens benefit not just from linearization (approximate the MLP cheaply) but from outright bypass (the MLP’s contribution is noise).

N2123 is diagnostic, not causal. Zeroing N2123 alone has no measurable effect on perplexity (<0.1% across all consensus levels), nor does clamping it ON for consensus tokens. The computation is genuinely distributed across 3072 neurons: N2123 is a reliable indicator of consensus breakdown—a vote-counter display—but removing the display does not change the election. This is consistent with the quorum system framing: in a 3072-voter system, no single voter is a bottleneck.

5 Discussion

5.1 The Smooth Function Framing, Revisited

There is a large body of productive work investigating the continuous and polynomial properties of neural network computation. Our results do not overturn this work; they suggest a complementary perspective. The signals flowing through the MLP are continuous—768-dimensional vectors with graded magnitudes. But the decision of *what to do with those signals* is binary: route them through the full nonlinear computation, or pass them through with minimal modification. When one examines MLP layers through this routing lens—binarizing activations and looking at co-firing patterns—an interpretable schematic of the routing logic emerges.

Return to the infinity symbol analogy. The smooth function framing predicts that the crossing should be resolved by separate smooth branches, recoverable by clustering. Our branch detection experiments found no such branches. The crossing is instead resolved by a binary routing decision: upper or lower, implemented by complementary neuron activations. The signal on each branch remains continuous; only the routing is discrete.

The ∞ exception illustrates the boundary: paragraph breaks trigger a single, consistent routing pattern—one condition with one outcome—that happens to be well-approximated by a low-degree polynomial. For any token class requiring multiple interacting routing conditions, the polynomial approximation breaks down, while the binary routing description remains interpretable.

5.2 Why Might Discrete Structure Emerge?

A natural question is why gradient descent—a continuous optimization process operating on a differentiable architecture—would converge on discrete switching patterns rather than smooth functions. We offer a speculative account, not a proof.

The residual stream is a representational bottleneck: 768 dimensions carrying thousands of superposed features [Elhage et al., 2022]. The MLP must make reliable routing decisions in this medium. Shannon’s information theory [Shannon, 1948] established that reliable signaling over a noisy channel benefits from discretization: snapping to distinguishable levels makes errors detectable rather than silently compounding.

An analogous pressure may operate here. If the MLP’s task is to route continuous signals to different processing based on context, binary routing decisions provide robustness that smooth interpolation does not: a neuron that is cleanly ON or OFF produces a reliable routing signal even when the input is noisy from superposition. GELU’s smoothness enables clean transitions between the two regimes—it makes the routing differentiable for training—but the trained network exploits the flat regions, not the transition zone.

This account is consistent with a broader pattern: biological neurons converged on all-or-nothing action potentials in a continuous electrochemical medium; digital circuits use continuous transistor physics to implement discrete logic. In each case, a continuous substrate supports discrete computation. Whether this parallel is deep or merely suggestive is an open question.

5.3 Beyond Shannon: When Both Matter

In Shannon’s relay circuits, the continuous signal (current) carried no computational information—it was pure substrate. Five milliamps and fifty milliamps both meant ON. Shannon could therefore characterize the computation entirely in terms of switching patterns and discard the analog properties. The analog computing tradition took the opposite position: continuous values *are* the computation, and discretization discards information.

The MLP is neither. Our binary-vs-continuous comparison (§4) reveals that binarization preserves the *routing* decision with essentially no loss (79.2% vs. 78.8% accuracy for predicting which tokens need nonlinear processing), but continuous activation magnitudes carry substantial additional information about *how much* correction to apply ($R^2 = 0.36$ vs. 0.22 for predicting output norm). You cannot reduce the MLP to pure switching logic—you would lose the magnitude information that determines the size of the nonlinear correction. But you equally cannot treat it as a smooth function approximator—polynomials fail catastrophically (§3).

The MLP is a **hybrid** system: binary routing of continuous signals, where the routing logic determines *whether* nonlinear processing occurs and the continuous magnitudes determine *what* that processing computes. This suggests that the productive question about MLP computation is not “is it discrete or continuous?” but rather “which aspects of the computation are discrete and which are continuous?” In GPT-2 Small, the answer is clear: the routing is discrete; the signal is continuous; both are essential. Whether this decomposition holds at larger scales remains an open empirical question.

5.4 The MLP as a Learned Quorum System

The consensus architecture resembles a **quorum system** from distributed computing: a set of voters must agree for a default action to proceed. When quorum is met, the 3072 neuron votes approximately cancel—the MLP’s net output is small and its residual effect is diffuse noise (Table 8: correct-token boost drops below $1.0\times$ from 4/7 onward). When quorum fails, the votes stop canceling, the net output is large and specific, and the result genuinely depends on which neurons fired.

Geva et al. [2021] characterized MLP layers as “key–value memories,” where each neuron stores a key (input pattern) and value (output direction). Our findings refine this: the default neurons are keys that match *most* inputs, producing values that cancel. The exception handler is a key that matches *only when the other keys disagree*—a meta-key that detects the failure of normal memory retrieval. Dai et al. [2022] identified “knowledge neurons” responsible for specific facts; our exception handler is not a knowledge neuron but a *routing* neuron—it doesn’t encode knowledge, it detects when knowledge retrieval is ambiguous.

5.5 Connection to Superposition and Polysemy

Polysemous tokens—those with multiple context-dependent meanings—exist in superposition within the residual stream [Elhage et al., 2022]. The consensus architecture provides a natural mechanism for resolving this:

- **Consensus holds** → the context is clear enough that the dominant sense suffices. Linear processing is adequate.
- **Consensus breaks down** → multiple senses are plausible. The exception handler fires and the MLP’s binary routing logic disambiguates.

This predicts that polysemous tokens should disproportionately trigger the exception handler—which is exactly what we observe: the top tokens when N2123 fires are function words, prepositions, and punctuation (“a”, “;”, “the”, “to”, “of”, “that”), all of which are highly polysemous.

5.6 Implications for Linearization

Prior work has shown that $\sim 50\%$ of MLP computation can be linearized at zero perplexity cost [Balogh, 2026a]. The binary routing framing provides a cleaner interpretation: for those tokens, the routing decision evaluates to “pass through”—the continuous signal needs no nonlinear processing. The mechanism analysis (Table 8) supports this: the MLP’s correct-token boost drops below $1.0\times$ from $4/7$ consensus onward, meaning its residual intervention at consensus is diffuse noise rather than useful computation. The “waste” is not failed approximation of a curve; it is a routing decision that selects the linear path, where the MLP’s contribution is at best negligible and at worst mildly harmful.

This suggests a principled linearization strategy: read the routing decision from the binary neuron activations, and skip the MLP for consensus tokens. The effect sizes are modest ($0.85\times$ to $1.15\times$ boost range), but the direction is consistent and the perplexity impact is clear ($4\times$ causal gradient). Unlike gate-based approaches that must learn routing from scratch, this leverages the routing structure already present in the weights.

5.7 Connections to Mixture-of-Experts

MoE architectures route tokens to different expert MLPs via an explicit gating function. Our findings suggest that *within* a single MLP, similar routing already occurs—not through explicit gating, but through the implicit binary routing logic of neuron activations. Each conjunction of active neurons selects a computational path for the continuous signal. N2123’s role as consensus monitor parallels MoE’s load-balancing mechanism: it detects tokens where the default routing (the linear path) is insufficient and activates the full nonlinear computation. The difference is that MoE routes between discrete experts, while the MLP routes between the linear default and a context-specific nonlinear correction—binary routing of a single continuous signal rather than selection among multiple processing units.

5.8 Generalization and Limitations

Within GPT-2 Small, the consensus structure is present in 6 of 12 layers (L0 and L7–11), with a developmental arc from single gateway neurons (L1–3) through diffuse processing (L4–6) to full consensus/exception quorums (L7–11) (Table 6). The detailed case study of Layer 11 is the cleanest instance of an architecture that crystallizes through depth, not an isolated anomaly. The absence of consensus in the middle layers is itself informative: it suggests that binary routing is not a universal organizational principle but rather emerges where the computational demands—measured by nonlinearity delta—are highest.

Across model scales, the picture is more limited. We ran identical analyses on GPT-2 Medium (345M, 24 layers, 4096 hidden) and GPT-2 Large (774M, 36 layers, 5120 hidden). The clean single-exception-handler pattern does not replicate at larger scales. Medium’s Layer 11 shows N2123 with a $1.0\times$ output norm ratio (no effect); Large’s Layer 11 shows near-degenerate $r > 0.98$ correlations among top neurons.

The question of how binary routing logic *organizes* at larger scales—whether through distributed consensus, multiple specialized handlers, or qualitatively different architectures—remains open and is the most important direction for future work.

The capacity hypothesis. A natural null hypothesis is that clean binary routing is an artifact of limited capacity: a 3072-neuron MLP may be *forced* into sharp switching because it lacks the width for smoother alternatives, and the pattern disappears precisely when capacity increases. This is consistent with the data—GPT-2 Medium (4096 hidden) and Large (5120 hidden) show weaker or absent consensus gradients. If correct, binary routing would be a compression strategy rather than an organizational principle, interesting for understanding small models but not predictive of larger ones. Distinguishing these accounts would require testing whether the pattern strengthens in even smaller models (e.g., width-reduced GPT-2 variants) and whether it re-emerges in larger models

under capacity pressure (e.g., after pruning). We leave this to future work but flag it as the most important alternative explanation for our findings.

The absence of models beyond the GPT-2 family is a further limitation. Architectures using SwiGLU or GeGLU activations [Shazeer, 2020] may exhibit different switching dynamics, and we cannot generalize beyond the GELU-based models studied here.

Semantic labels. The role labels in Table 3 (“general punctuation,” “subordinate clauses,” etc.) are post-hoc descriptions based on inspecting the highest-firing tokens for each neuron. They are suggestive but not independently validated—a proper validation would cross-reference against an external POS tagger or compare to sparse autoencoder features. We retain them as interpretive aids but caution against treating them as established facts.

6 Related Work

Mechanistic interpretability. Our work connects to the circuits research program [Olah et al., 2020, Elhage et al., 2021], which identifies computational motifs in neural networks.

Relationship to sparse autoencoders. SAEs [Bricken et al., 2023, Cunningham et al., 2023] decompose activations into interpretable features—they answer *what* each neuron or direction represents. Public SAE decompositions of GPT-2 Small exist [Gao et al., 2024, Bloom, 2024] and could in principle identify features corresponding to our consensus neurons. Our work asks a different question: not what individual neurons represent, but how their *joint activation patterns* determine computational routing. The consensus gradient, mutual exclusivity structure, and causal importance prediction are *relational* properties between neurons that SAE decomposition does not extract—an SAE might label N2123 as “ambiguous syntactic context” but would not reveal that it is 93–98% exclusive with 7 specific other neurons whose agreement monotonically predicts MLP importance. The two approaches are complementary: SAEs characterize the feature vocabulary; binary routing analysis characterizes the grammar that connects features to computation.

MLP function. Geva et al. [2021] showed that MLP layers act as key–value memories; our routing framing extends this by characterizing the *retrieval mechanism* as binary routing rather than soft matching. Dai et al. [2022] studied knowledge neurons; N2123’s role as an exception handler suggests a higher-level organizational principle above individual knowledge storage.

Spline theory. Balestriero & Baraniuk [2018] established that deep networks with piecewise-linear activations are continuous piecewise-affine spline operators, connecting neural networks to classical approximation theory. This characterizes the *mechanism*: the network partitions input space into polytopes with affine maps. Our work asks a complementary question about the *computation*: along the natural data manifold, do those partition boundaries reflect smooth variation or discrete decisions? We find evidence for the latter in GPT-2 Small, though we emphasize that our results are compatible with, not contradictory to, the spline framework.

Quantization and sparsity. Dettmers et al. [2022] showed that transformer weights exhibit emergent outlier features at scale—single dimensions with magnitudes 5–20× larger than the rest—that dominate quantization error. This is complementary to our finding: outlier features concern *weight magnitude* along specific dimensions, while binary routing concerns *activation patterns* across neurons. Both suggest that transformers organize computation around a small number of high-impact features rather than distributing it uniformly.

Linearization. Efforts to linearize or prune transformer components [Sharma et al., 2024, Men et al., 2024] typically treat the MLP as a black box to be approximated. Our results suggest an additional angle: rather than asking “what curve does the MLP compute?” one might ask “which tokens are routed to the nonlinear path?” and linearize only the rest.

Gating and conditional computation. The fast-path / slow-path structure we identify in Layer 11 echoes adaptive computation time [Graves, 2016] and early exit strategies [ElBayad et al., 2020], but emerging naturally from standard training rather than being architecturally imposed. SwiGLU and GeGLU [Shazeer, 2020] make gating explicit in the architecture; our findings suggest that GELU-based MLPs learn implicit gating from standard training.

Discrete structure in neural networks. Nanda et al. [2023] showed that grokking in modular arithmetic produces clean, interpretable circuits—discrete algorithmic structure emerging from

gradient descent. The lottery ticket hypothesis [Frankle & Carbin, 2019] demonstrates that sparse subnetworks carry the essential computation. Both are consistent with the view that trained networks converge on discrete structure despite continuous parameterization.

7 Conclusion

We set out to test whether MLP nonlinearity in transformers has smooth polynomial structure, and to characterize what structure it does have.

The polynomial probing results are clear: across degrees 2–7, five clustering methods, and context augmentation, no smooth structure emerges in the nonlinear residual. This holds even when we allow multiple subpopulations with different polynomial forms. The one exception—paragraph boundaries—is a single-condition switching pattern that happens to be trivially polynomial.

The binary feature characterization offers a complementary lens. In GPT-2 Small’s Layer 11, binarized neuron activations reveal an exception-handler circuit with 93–98% mutual exclusivity, a perfectly monotonic consensus gradient across eight levels, and a $2.8\times$ output norm ratio. This structure goes well beyond what marginal firing rates predict under independence, and it is interpretable as discrete routing logic. Critically, this is not an isolated finding: a cross-layer analysis at 500K tokens reveals a three-phase developmental arc—scaffold layers (L0–3) with gateway routing, diffuse layers (L4–6) with distributed processing, and decision layers (L7–11) where the full consensus/exception architecture crystallizes with increasing quorum complexity (1→3→7 consensus neurons, 85–98% exclusivity).

Causal validation confirms that the consensus structure predicts functional importance: removing the MLP costs 43.3% perplexity at consensus breakdown but only 10.1% at full consensus—a $4\times$ difference. The mechanism analysis reveals a dissociation: the MLP reshapes the full output distribution substantially at breakdown (KL = 0.414) but this effect is primarily distributional, not concentrated on the correct token (boost = $1.15\times$). At consensus, even this distributional contribution fades to noise (boost < $1.0\times$).

We are candid about the remaining limitations: the consensus pattern does not replicate cleanly at larger model scales (GPT-2 Medium and Large), and the Shannon analogy is an interpretive lens rather than a formal isomorphism. But the core observations—that MLP neurons operate in near-binary regimes, that their co-activation patterns carry structure far exceeding independence baselines, and that this structure predicts which tokens require nonlinear processing—hold across all layers of GPT-2 Small and may generalize further.

There is beautiful and productive work characterizing neural networks as continuous function approximators. We suggest that when one looks instead at the routing decisions—which tokens get nonlinear processing and which pass through linearly—one finds an additional layer of interpretable structure: binary routing of continuous signals, implemented by continuous machinery.

References

- Peter Balogh. Half the nonlinearity is wasted: The wanamaker effect in transformer MLP layers. Working paper, 2026.
- Peter Balogh. Shooting the swordsman: Selective linearization of transformer MLP layers. Working paper, 2026.
- Randall Balestriero and Richard G. Baraniuk. A spline theory of deep learning. In *International Conference on Machine Learning (ICML)*, 2018.
- Trenton Bricken, Adly Templeton, Joshua Batson, Brian Chen, Adam Jermyn, Tom Henighan, Tom Conerly, Nick Turner, Cem Anil, Carson Denison, Amanda Askell, Robert Lasenby, Yifan Wu, Shauna Kravec, Nicholas Schiefer, Tim Maxwell, Nicholas Joseph, Zac Hatfield-Dodds, Alex Tamkin, Karina Nguyen, Brayden McLean, Josiah E. Burke, Tristan Hume, Shan Carter, Tom Henighan, and Chris Olah. Towards monosemanticity: Decomposing language models with dictionary learning. *Transformer Circuits Thread*, 2023.

- Hoagy Cunningham, Aidan Ewart, Logan Riggs, Robert Huben, and Lee Sharkey. Sparse autoencoders find highly interpretable features in language models. *arXiv preprint arXiv:2309.08600*, 2023.
- Damai Dai, Li Dong, Yaru Hao, Zhifang Sui, Baobao Chang, and Furu Wei. Knowledge neurons in pretrained transformers. In *ACL*, 2022.
- Maha ElBayad, Jiatao Gu, Edouard Grave, and Michael Auli. Depth-adaptive transformer. In *ICLR*, 2020.
- Nelson Elhage, Neel Nanda, Catherine Olsson, Tom Henighan, Nicholas Joseph, Ben Mann, Amanda Askell, Yuntao Bai, Anna Chen, Tom Conerly, Nova DasSarma, Dawn Drain, Deep Ganguli, Zac Hatfield-Dodds, Danny Hernandez, Andy Jones, Jackson Kernion, Liane Lovitt, Kamal Ndousse, Dario Amodei, Tom Brown, Jack Clark, Jared Kaplan, Sam McCandlish, and Chris Olah. A mathematical framework for transformer circuits. *Transformer Circuits Thread*, 2021.
- Nelson Elhage, Tristan Hume, Catherine Olsson, Nicholas Schiefer, Tom Henighan, Shauna Kravec, Zac Hatfield-Dodds, Robert Lasenby, Dawn Drain, Carol Chen, Roger Grosse, Sam McCandlish, Jared Kaplan, Dario Amodei, Martin Wattenberg, and Christopher Olah. Toy models of superposition. *Transformer Circuits Thread*, 2022.
- Mor Geva, Roei Schuster, Jonathan Berant, and Omer Levy. Transformer feed-forward layers are key-value memories. In *EMNLP*, 2021.
- Alex Graves. Adaptive computation time for recurrent neural networks. *arXiv preprint arXiv:1603.08983*, 2016.
- Xin Men, Mingyu Xu, Qingyu Zhang, Bingning Wang, Hongyu Lin, Yaojie Lu, Xianpei Han, and Weipeng Chen. ShortGPT: Layers in large language models are more redundant than you expect. *arXiv preprint arXiv:2403.03853*, 2024.
- Stephen Merity, Caiming Xiong, James Bradbury, and Richard Socher. Pointer sentinel mixture models. *arXiv preprint arXiv:1609.07843*, 2016.
- Chris Olah, Nick Cammarata, Ludwig Schubert, Gabriel Goh, Michael Petrov, and Shan Carter. Zoom in: An introduction to circuits. *Distill*, 2020.
- Alec Radford, Jeff Wu, Rewon Child, David Luan, Dario Amodei, and Ilya Sutskever. Language models are unsupervised multitask learners. 2019.
- Claude E. Shannon. A mathematical theory of communication. *Bell System Technical Journal*, 27(3):379–423, 1948.
- Claude E. Shannon. A symbolic analysis of relay and switching circuits. *Transactions of the AIEE*, 57(12):713–723, 1938.
- Noam Shazeer. GLU variants improve transformer. *arXiv preprint arXiv:2002.05202*, 2020.
- Pratyusha Sharma, Jordan T. Ash, and Dipendra Misra. The truth is in there: Improving reasoning in language models with layer-selective rank reduction. In *ICLR*, 2024.
- Neel Nanda, Lawrence Chan, Tom Lieberum, Jess Smith, and Jacob Steinhardt. Progress measures for grokking via mechanistic interpretability. In *ICLR*, 2023.
- Leo Gao, Tom Dupré la Tour, Henk Tillman, Gabriel Goh, Rajan Troll, Alec Radford, Ilya Sutskever, Jan Leike, and Jeffrey Wu. Scaling and evaluating sparse autoencoders. *arXiv preprint arXiv:2406.04093*, 2024.
- Joseph Bloom. Open source sparse autoencoders for all residual stream layers of GPT-2 Small. *Alignment Forum*, 2024.
- Tim Dettmers, Mike Lewis, Younes Belkada, and Luke Zettlemoyer. LLM.int8(): 8-bit matrix multiplication for transformers at scale. In *NeurIPS*, 2022.
- Jonathan Frankle and Michael Carbin. The lottery ticket hypothesis: Finding sparse, trainable neural networks. In *ICLR*, 2019.

A Two Regimes Data

Table 9: **Two Regimes (Layer 11)**. N2123 firing rate and MLP output norm as a function of consensus neuron count (N2, N2361, N2460, N2928, N1831, N1245, N2600). 500K WikiText-103 tokens, GPT-2 Small.

Consensus	Count	%	N2123 Fire Rate	Avg MLP output
0 / 7	11,358	2.3%	94.7%	194.1
1 / 7	19,131	3.8%	83.6%	155.5
2 / 7	19,142	3.8%	56.5%	126.1
3 / 7	26,189	5.2%	24.4%	102.4
4 / 7	53,042	10.6%	10.3%	88.6
5 / 7	95,267	19.1%	4.5%	82.3
6 / 7	146,070	29.2%	1.4%	76.2
7 / 7	129,513	25.9%	0.5%	70.0

B Generalization Data

Note on neuron indexing. For Medium and Large, we test the same neuron *index* (2123) and consensus neuron indices as in GPT-2 Small. These are different neurons with different learned weights; the uniform $\sim 2\%$ firing rate confirms that the specific consensus/exception structure does not transfer across model scales by index alone. A full re-discovery of each model’s own exception handler is left to future work.

Table 10: Two Regimes consensus table for GPT-2 Medium Layer 11 (4096 hidden neurons, 200K tokens). The monotonic gradient is absent; neuron 2123 fire rate is uniformly low ($\sim 2\%$).

Consensus	Count	%	N2123 Fire Rate	Avg Norm
0 / 7	116,024	58.0%	1.7%	25.6
1 / 7	70,100	35.1%	1.9%	25.3
2 / 7	12,312	6.2%	2.7%	26.9
3 / 7	1,408	0.7%	2.2%	27.7

Table 11: Two Regimes for GPT-2 Large Layer 35 (5120 hidden, 200K tokens). A mild gradient exists but is far weaker than GPT-2 Small.

Consensus	Count	%	N2123 Fire Rate	Avg Norm
0 / 7	115,182	57.6%	1.6%	40.8
1 / 7	67,693	33.9%	3.0%	43.7
2 / 7	14,941	7.5%	5.4%	46.6
3 / 7	1,945	1.0%	10.1%	47.0
4 / 7	168	0.1%	8.3%	48.8

C Hyperparameter Sensitivity

The result is stable: R^2 remains near 0.04 regardless of PCA dimensionality or regularization strength, confirming that the polynomial failure is not an artifact of hyperparameter choices.

Table 12: Polynomial R^2 sensitivity to PCA dimensions and Ridge α (Layer 9, degree 3, 100K tokens, cross-validated). The result is stable: no configuration exceeds $R^2 = 0.07$.

PCA dims	$\alpha = 0.1$	$\alpha = 1$	$\alpha = 10$	$\alpha = 100$
10	0.038	0.039	0.037	0.029
20	0.042	0.043	0.040	0.031
50	0.041	0.041	0.038	0.030
100	0.039	0.038	0.035	0.028